Available online at www.sciencedirect.com

SciVerse ScienceDirect

Ceramics International 39 (2013) 7305–7315

CERAMICS INTERNATIONAL

www.elsevier.com/locate/ceramint

# Microstructure and ionic conductivity properties of gadolinia doped ceria ($Gd_xCe_{1-x}O_{2-x/2}$) electrolytes for intermediate temperature SOFCs prepared by the polyol method

M.A. Faruk Öksüzömer*, Göknur Dönmez, Vedat Sariboğa, Tuba Gürkaynak Altinçekiç

*Department of Chemical Engineering, Istanbul University, 34320 Avalar, Istanbul, Turkey*

Received 11 January 2013; received in revised form 20 February 2013; accepted 21 February 2013
Available online 27 February 2013

**Abstract**

$Gd_{0.1}Ce_{0.9}O_{1.95}$ and $Gd_{0.2}Ce_{0.8}O_{1.9}$ powders were prepared through the polyol process without using any protective agent. Microstructural and physical properties of the samples were characterized with X-ray diffraction (XRD), scanning electron microscopy (SEM), thermogravimetry (TG) and impedance analysis methods. The results of the thermogravimetry/differential thermal analysis (TG/DTA) and XRD indicated that a single-phase fluorite structure formed at the relatively low calcination temperature of 500 °C. The XRD patterns of the samples revealed that the crystallite size of the samples increased as calcination temperatures increased. The sintering behavior and ionic conductivity of pellets prepared from gadolinia doped ceria (GDC) powders, which were calcined at 500 °C, were also investigated. The relative densities of the pellets, which were sintered at temperatures above 1300 °C, were higher than 95%. The results of the impedance spectroscopy revealed that the GDC-20 sample that was sintered at 1400 °C exhibited an ionic conductivity of $3.25 \times 10^{-2}$ S cm$^{-1}$ at 800 °C in air. This result clearly indicates that GDC powder with adequate ionic conductivity can be prepared through the polyol process at low temperatures.


*Keywords:* C. Ionic conductivity; E. Fuel cells; Polyol method; Doped-$CeO_2$

## 1. Introduction

Fuel cells are becoming an increasingly viable source of power for many applications due to a growing demand for economical and clean electrical energy. Several types of fuel cell systems that operate at varying temperatures and efficiencies are currently available [1]. Among all of the fuel cell systems, solid oxide fuel cells (SOFCs) have gained considerable attention as promising systems for electrical power generation because of their high conversion efficiency for transforming chemical energy to electric power. Furthermore, SOFCs have the advantage of fuel flexibility, and the capability of working with hydrogen, hydrocarbon reformate and, in some circumstances, directly with hydrocarbon fuels [2].

Solid oxide fuel cells are classified into two groups according to their operation temperature: high temperature solid oxide fuel cells (HT-SOFCs) and intermediate temperature solid oxide fuel cells (IT-SOFCs). Although some researchers focus on developing HT-SOFCs, reducing the operation temperature of fuel cells is important for achieving long-term performance stability and for reducing the cost of materials processing and cell fabrication. To reduce the operation temperature, two approaches are widely applied that lower the resistance of dense electrolyte membranes: decreasing the traditional YSZ (8 mol %$Y_2O_3$–$ZrO_2$) electrolyte thickness or using alternative materials with higher conductivity at lower temperatures [3].

Doped ceria electrolytes are good candidates for SOFCs at intermediate temperatures despite their high ionic conductivity and low activation energy and stability within

*Corresponding author. Tel.: +90 212 440 00 00/17652.
*E-mail address:* fufu@istanbul.edu.tr (M.A.F. Öksüzömer).

0272-8842/$ - see front matter © 2013 Elsevier Ltd and Techna Group S.r.l. All rights reserved.
http://dx.doi.org/10.1016/j.ceramint.2013.02.069

the temperature range of room temperature to its melting point (approximately 2300 °C). The ceria is either doped with $Gd^{+3}$ or $Sm^{+3}$, both of which have slightly higher ionic radii than $Ce^{+4}$ ions. Because the ionic radii of Gd and Sm are nearly the same as the ionic radii of cerium, their incorporation in ceria lattice for creating more oxygen ion vacancies produces less distortion in host lattices and, thereby prevents phase instability. These excess oxygen vacancies generally yield a higher ionic conductivity of oxygen and higher electronic conductivity than un-doped ceria, due to the reduction of the cerium ion from the tetravalent state to the trivalent state at high temperatures in a reducing atmosphere [4,5]. Because of their high ionic conductivity at relatively moderate temperatures, these materials have great potential as electrolytes for SOFCs at intermediate temperatures. Gadolinia doped ceria is one of the most promising electrolytes for SOFCs that operate below 650 °C [6,7].

To synthesize ceria-based electrolytes with the desired properties, various methods such as hydrothermal synthesis [8,9], homogenous precipitation [10,11], the sol-gel process [12], the glycine-nitrate process [13], combustion [14], the reverse microemulsion process [15], and a variant of the sol-gel process known as cation complexation [16] have been employed.

Among the several chemical methods for preparing metal particles, a solvothermal route has been considered as a promising method to obtain monodispersed metal particles. In this procedure, polyalcohols with high boiling points and the ability to solve organic salts at elevated temperatures are utilized. Ethylene glycol and triethylene glycol are a few examples of these compounds; 'polyol' is a general term for polyalcohols. To prepare metal particles, the polyol process was applied because of its mild reducing properties and simple route. In addition, polyol acts as a solvent with a chelating effect, which prevents the agglomeration of particles during reaction. Powders obtained from the polyol method exhibit homogenous phase composition, narrow particle distribution and highly specific surface areas. Due to its simplicity and numerous advantages, the polyol method has received considerable attention regarding the preparation of highly pure mixed oxides [17,18].

The oxygen ion conductivity of solid solutions of GDC, typically with 10–20% substitution of Ce with Gd, is one of the highest conductivities in this class of solid electrolytes [19,20].

A solvothermal route, which is a low-cost and relatively simple method, was used in the preparation of 10% and 20% mole GDC. No sintering aids (transition metal oxides such as $MnO_2$) [21] or protective agents were used. The effect of calcination temperature on the crystal structure of GDCs was investigated. The crystallite sizes were determined by X-ray diffraction analysis (XRD) and the sample densities were measured by Archimedes' method after sintering. The thermal decomposition behavior of the samples was also evaluated by using thermal gravimetric analysis. The microstructural features and the ionic conductivity values of the samples were characterized by scanning electron microscopy (SEM) studies and impedance spectroscopy measurements, respectively.

## 2. Experimental analysis

### 2.1. Preparation of GDC powders

Cerium (III) acetate hydrate ($(C_2H_3O_2)_3Ce \cdot xH_2O$, 99.9% metal basis, Aldrich) and gadolinium (III) acetate hydrate ($(C_2H_3O_2)_3Gd \cdot xH_2O$, 99.9% metal basis, Aldrich) were used as metal precursors and triethylene glycol (TREG)($C_6H_{14}O_4$, Merck) was used as a solvent and reducing agent. In the polyol process, the specified amounts of metal precursors were dissolved in 100 ml triethylene glycol. The total ion concentration was maintained at 0.2 M. The solution was transferred to a 250 ml three-neck spherical glass flask equipped with a refluxing condenser and thermometer and placed on a magnetic stirrer. The synthesized powders were labeled according to the mole percent of gadolinium that was used in the process: GDC-10 and GDC-20. All experimental conditions for GDC-10 and GDC-20 were equivalent. First, the metal precursors were dissolved in the reducing agent at 60–80 °C; the solution was then heated to 200 °C and maintained at this temperature approximately 3 h under vigorous stirring. During this time, the color of the reaction mixture changed from white to yellow and then to dark brown. The reaction solution was subsequently cooled to room temperature and the solids were separated by centrifugation and washed with ethanol and de-ionized water.

The solids were dried at 70 °C. The conversion of the prepared amorphous precursors to crystalline gadolinia-doped $CeO_2$ was achieved by heating the dried solid gels at a heating rate of 5 °C $min^{-1}$ to temperatures of 500 °C, 750 °C, 1000 °C and maintaining these temperatures for 4 h. Because the calcination performed at 500 °C for 4 h was sufficient enough to obtain crystalline gadolinia-doped ceria, all solid samples were calcined at this temperature. The flow chart of the polyol process is given in the Fig. 1.

### 2.2. Characterization of the powders

#### 2.2.1. Thermal analysis

The thermal behavior of the prepared GDC-10 and GDC-20 powders was analyzed with SII Exstar 6000 TG/DTA 6300 from 40 °C to 1000 °C at a constant heating rate of 10 °C $min^{-1}$ under air. The results of the TG and DTA were plotted as a function of temperature.

#### 2.2.2. X-ray analysis and crystallite size determination

The XRD technique was used to examine the crystalline structure and phase purity. Calcined powders were studied by XRD using a Rigaku D/max-2200 Ultima X-ray diffractometer with CuKα radiation. Data in an angular

region of $2\theta = 20$–$90^\circ$ were collected. From the X-ray diffractograms, phases and average crystallite sizes, $D$, of the $Ce_{1-x}Gd_xO_{2-x/2}$ samples were calculated from X-ray line broadening of the reflections of (1 1 1) by using the well-known Scherrer equation:

$$D = \frac{0.9\lambda}{\beta \cdot \cos\theta} \quad (1)$$

where $\lambda$ is the wavelength of the X-rays (1,5418 Å), $\theta$ is the scattering angle of the main reflection (1 1 1) and $\beta$ is the corrected peak at full width at half maximum (FWHM) intensity. The lattice parameter of the doped ceria's was calculated by the relation:

$$a = d\sqrt{h^2 + k^2 + l^2} \quad (2)$$

where $a$ is the cubic lattice parameter; $d$ is the spacing between the planes in the atomic lattice, which is calculated by Bragg's law and $h$, $k$ and $l$ are the miller indices of the plane.

#### 2.2.3. Density determination

The calcined powders were pressed with a cold isostatic press (CIP) at 200 MPa to obtain a disc-shaped test sample. The compact disc samples were then sintered at different temperatures (1100 °C, 1200 °C, 1300 °C, 1400 °C and 1500 °C) for 6 h. The densities of the sintered discs were determined by Archimedes' method:

$$d_{pellet} = \frac{W.\rho}{W_1 - W_2} \quad (3)$$

where $W$ is the dry weight, $W_1$ is the wet weight, $W_2$ is the body's submerged weight without fine wire and $\rho$ is the density of solvent (ethanol at 26 °C with a density of 0.785 g $cm^{-3}$). After determination of the bulk density, the relative densities of the samples were calculated by dividing the experimental bulk density values by the theoretical densities. The theoretical densities of the samples were taken as 7.21 g $cm^{-3}$ and 7.23 g $cm^{-3}$ for GDC-10 and GDC-20, respectively, which were calculated by using the lattice parameters obtained from the XRD analysis: $a = 5.421$ Å for GDC-10 and $a = 5.427$ Å for GDC-20.

#### 2.2.4. Scanning electron microscopy (SEM) analysis

The samples were placed on stubs using carbon tape and then coated with Au to avoid particle charging. The scanning electron micrographs were obtained by using FEI Quanta FEG scanning electron microscopy to identify the morphology and microstructure of the sintered samples.

#### 2.2.5. Oxygen conductivity measurements

Initially, both sides of the sintered pellets were covered with Ag paste and maintained at 800 °C for half an hour. The ionic conductivity measurements of the sintered pellets, which were 11–12 mm in diameter and 1–1.5 mm in thickness, were obtained with an AC impedance analyzer (Solartron 1260 FRA and 1296 interface) in the temperature range of 200–800 °C.

## 3. Results and discussion

### 3.1. TG/DTA analysis

The thermal analysis methods investigate the properties of solids as a function of temperature. They are useful for determining phase changes, decomposition, loss of water or oxygen, and for constructing phase diagrams. In TGA, the weight of a sample is monitored as a function of temperature at a controlled heating rate [22] .

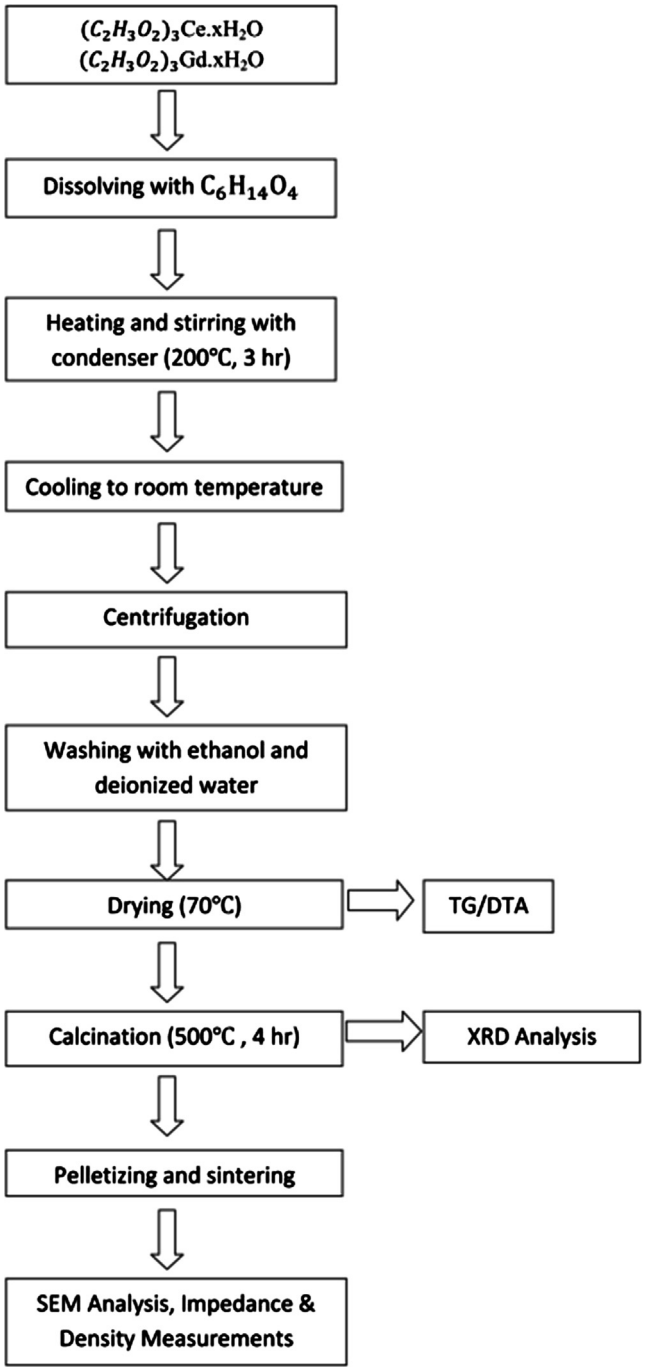


Fig. 1. Flow chart of the process.

The thermal decomposition behavior of $Gd_{0.2}Ce_{0.8}O_{1.9}$ powders is shown in Fig. 2. As seen in the figure, weight loss occurred in three steps. In the first step, a weight loss of 3.9% occurred due to the dehydration and decomposition of acetate groups in the temperature range of 40–196 °C. The next step, which is shown in Fig. 2 at 221 °C, corresponds to a weight loss of 14.3% and is related to the combustion of organic residues. A minor weight loss, which occurred between 221 °C and 435 °C, can be ascribed to the removal of residual triethylene glycol. Almost no remarkable weight change was detected above 500 °C on the TG curve, which suggests the formation of crystalline $Ce_{1-x}Gd_xO_{2-x/2}$. The XRD results, which will be discussed in the following section, also confirm these findings.

### 3.2. Powder characterization

X-ray diffraction is a versatile, non-destructive technique that reveals detailed information about the crystallographic structure of natural and manufactured materials. The phase evolution of the precursors upon calcination was determined by the method of XRD. The XRD patterns for the GDC powders that were calcined at 500 °C, 750 °C and 1000 °C are shown in Fig. 3. According to the results of XRD, crystallization of the powders occurred at 500 °C. These results indicate that the products consist of single phase $CeO_2$ with a cubic fluorite structure (JCPDS Card No:34-394). No peaks were detected for the gadolinium oxide. The results indicate that the dopant ion was fully substituted in the $CeO_2$ lattice. The calculated lattice parameters of the samples are 5.421 Å for GDC-10 and 5.427 Å for GDC-20, which indicate solid solution formation because pure ceria contains lattice parameters of 5.411 Å [23]. The reflection peaks became sharper and narrower with increased calcination temperatures, which indicates that the crystal sizes increase and the crystallinity of the powders becomes better-defined during the calcination process. However, after heating at 1000 °C, the width of the peaks' became very narrow and intensified, which indicates a rapid increase in the size of the crystallite.

The crystallite sizes, which were calculated from the Scherer equation, of the GDC-20 samples calcined at 500 °C, 750°C and 1000 °C consisted of 10.9 nm, 20.4 nm and 43.2 nm, respectively.

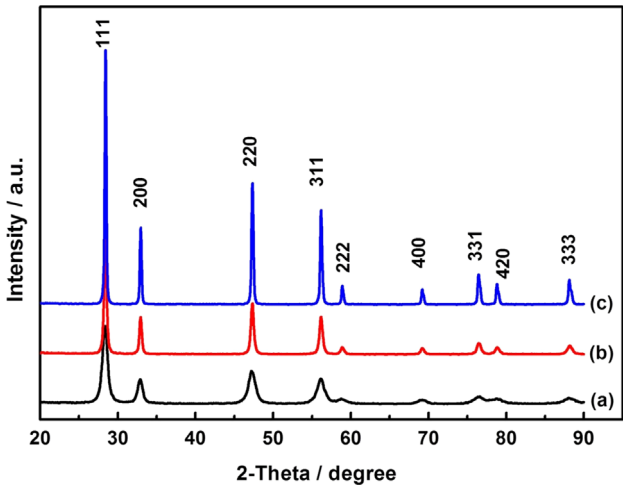


Fig. 3. XRD patterns of nanocrystalline $Gd_{0.2}Ce_{0.8}O_{1.9}$ powders calcined in air for 4 h at (a) 500 °C (b) 750 °C and (c) 1000 °C.

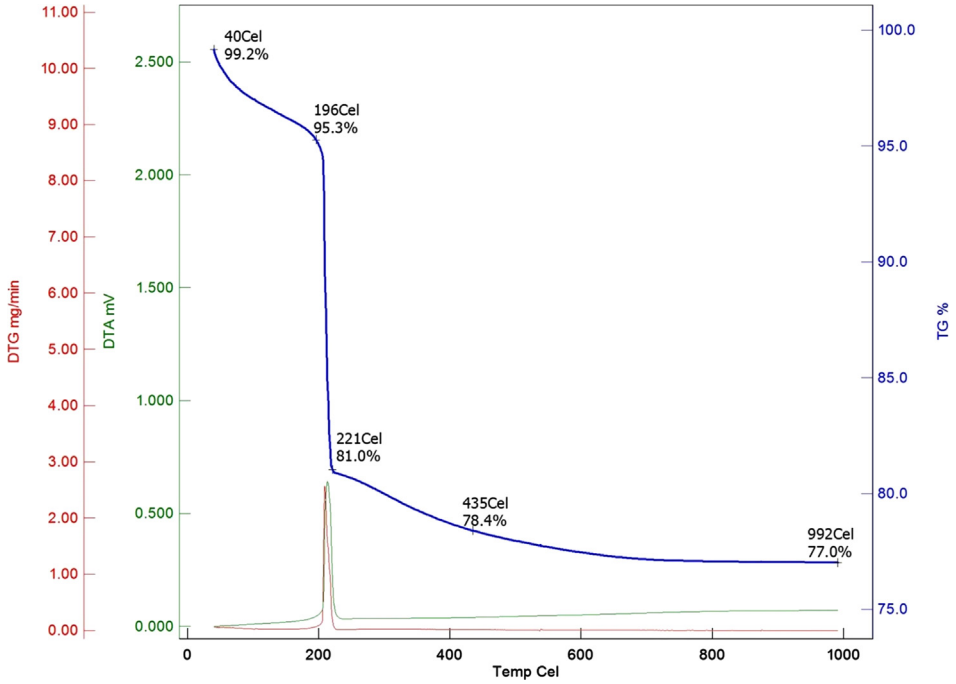


Fig. 2. TG/DTA curve of thermal decomposition of GDC-20 powder precursor at a heating rate of 10 °C $min^{-1}$ in dry air.

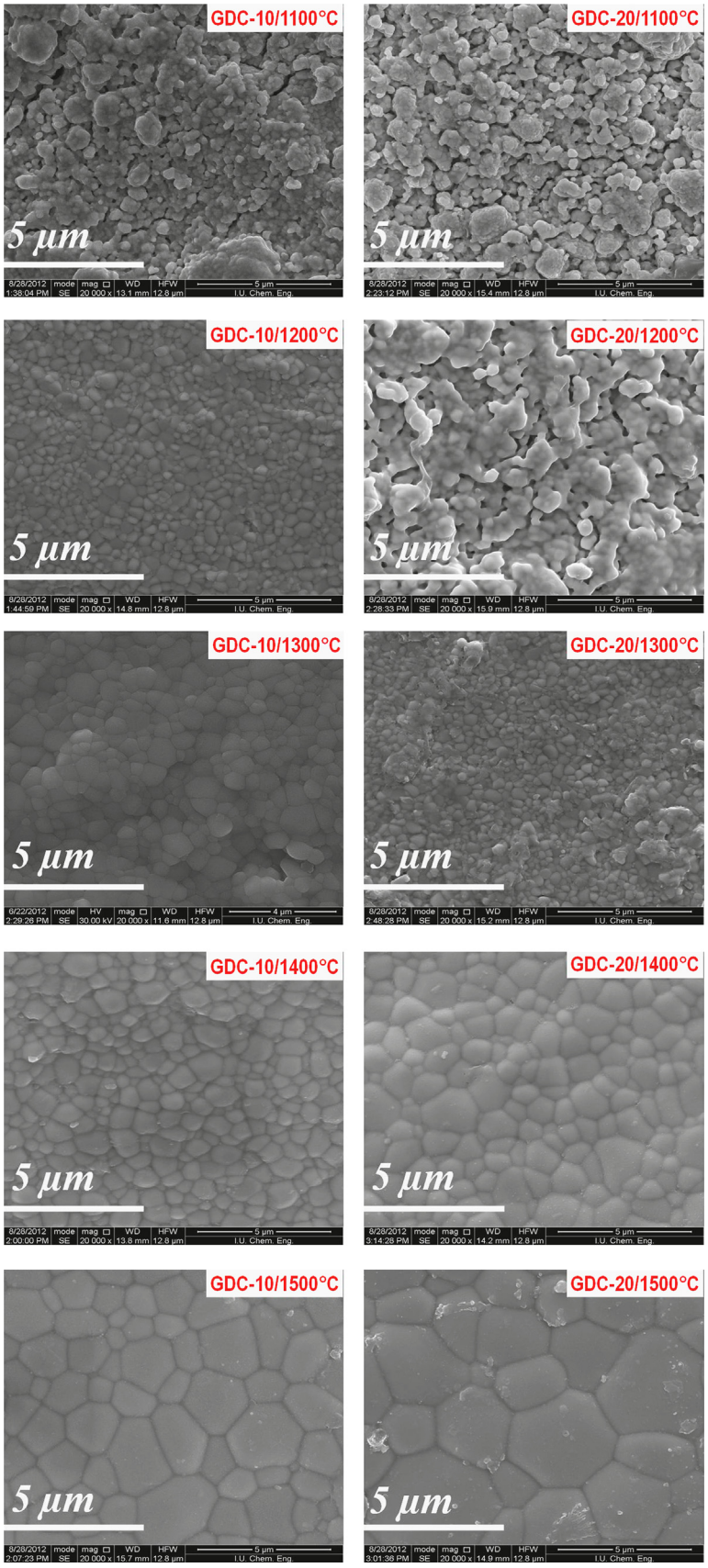


Fig. 4. Scanning electron micrographs of sintered GDC-10 and GDC-20 samples (20,000 ×).

As mentioned previously, no remarkable change was detected above 500 °C on the TG curve. As a result, the calcination operation at 500 °C was selected for all samples. Lower crystallite sizes typically provide higher density for ceramics [24].

### 3.3. Sintering and microstructures

Scanning electron microscopy was used to observe the morphological features and defects within the sample microstructure and to determine the distribution of elements [22]. The SEM images displayed in Fig. 4 show the effect of sintering temperature on density and grain growth. The samples that were sintered at higher temperatures were composed of nearly fully dense material, whereas the samples sintered at lower temperature were more porous. The densities of the pellets sintered at different temperatures were measured; GDC-10 and GDC-20 pellets contained 95% theoretical density at temperatures above 1300 °C. This value is comparatively higher than the values of the previously reported results [17,25]. The sintering behavior of two GDC groups is quite different. When compared with GDC-10, the GDC-20 group showed a retarded but rapid sintering at 1400 °C. Between 1100 and 1300 °C, GDC-10 exhibited larger grains. At 1400 °C, GDC-20 exhibited better grain growth in contrast with GDC-10. At a high magnification (40000 ×), the grain size increased when using the enhanced amount of dopant cations that were sintered at 1400 °C as illustrated in Fig. 5. Conversely, Suzuki et al. [26] reported that a higher content of dopant realized a smaller grain size. In addition, Chourasiya et al. [27] stated that grain size decreased with Gd concentration. In another study, Zhang et al. [28] indicated that there is no strong impact of Gd content on grain growth and densification, although a slight decrease was observed for both grain size and densification. As mentioned previously, the grain size of GDC-20 was higher than the grain size of the GDC-10 sample for the sintering operations at 1400 °C and 1500 °C.

The average grain sizes of the sintered samples were measured by using SEM images at higher magnifications; the results are provided in Table 1.

Electron dispersive X-ray analysis (EDX) provided an elemental analysis of the samples. The results of the elemental analyses of the GDC-10 and GDC-20 samples are shown in Fig. 6. The polyol microwave assisted method [17] was also used to synthesize nanocrystalline $Ce_{1-x}Gd_xO_{2-\delta}$ (GDC) particles but the as-synthesized powders contain a lower gadolinium amount than the theoretical value, which is most likely due to the formation of stable gadolinium diglycolate complexes that are derived from the interaction of diethylene glycol and nitric compounds. To overcome this problem, we began with acetate precursors of gadolinium and cerium and used triethylene glycol. As a result, we obtained the desired stoichiometry as confirmed by the Energy Dispersive X-ray Spectrometry (EDS) results. After thermal treatment in an oven at 500 °C for 4 h, the samples experienced a concominant weight loss of 23%. No further weight loss was detected after thermal treatment at 500 °C for 4 h. Therefore, the actual final reaction yield was 67% for $Gd_{0.1}Ce_{0.9}O_{1.95}$ and 55% for $Gd_{0.2}Ce_{0.8}O_{1.9}$.

### 3.4. Conductivity measurement

Electrochemical Impedance Spectroscopy uses electronically conducting electrodes to characterize the electrical properties of materials and their interfaces. The evaluation

Table 1
Average grain sizes (μm) of GDC samples obtained from SEM images.

| Sintering temperature (°C) | Compositions | |
|---|---|---|
| | GDC-10 (μm) | GDC-20 (μm) |
| 1100 | 0.62 | 0.45 |
| 1200 | 0.64 | 0.67 |
| 1300 | 0.80 | 0.71 |
| 1400 | 1.22 | 1.69 |
| 1500 | 2.50 | 2.93 |

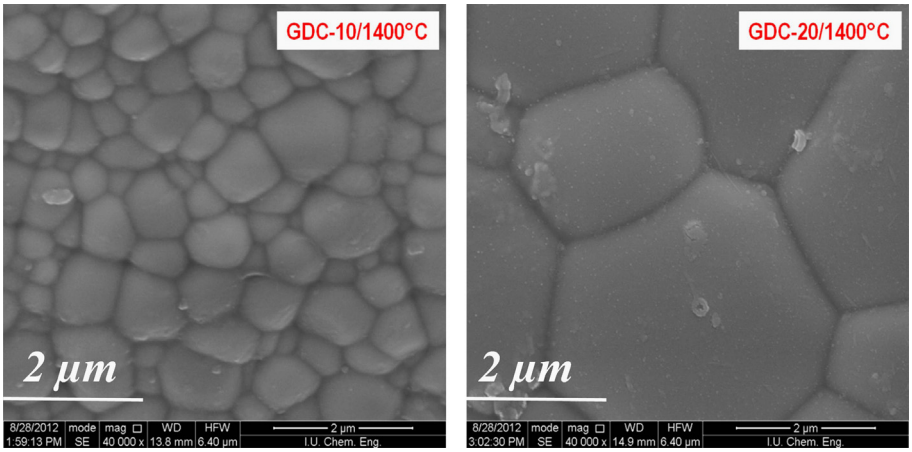


Fig. 5. Scanning electron microscopy images of GDC-10 and GDC-20 samples sintered at 1400 °C (40,000 ×).

of the electrochemical behavior of electrolyte and/or electrode materials is performed by applying voltage to electrodes and observing the response [29]. The use of impedance spectroscopy to determine the oxygen ionic conductivity was first introduced by Bauerle [30]. Solid oxide fuel cell electrolytes are oxygen ion conductors, therefore, they can be studied by using this technique. Impedance spectroscopy is essentially a technique that is employed in the study of mobile charges in ionic, semi-conducting or insulating solids, and is also used to measure the resistance, or the impedance, of the grain boundary, the grain and the electrode of a sample [1].

The impedance spectrum of an ionic conductor contains contributions from the grains, the grain boundary, and the electrode–electrolyte interface, which can be simplified by three arcs. However, depending on the nature of the sample and conditions of the experiment, not all of these arcs can be observed [31,32]. The three arcs can be identified clearly below 500 °C.

The ionic conductivity measurement was performed in air in the temperature range of 200–800 °C. A complex plane plot of real impedance, $Z'$, versus imaginary impedance, $Z''$, was prepared for each set of data. By curve fitting a circle to semicircles on these plots, sample resistances ($R$) were obtained. The total conductivity ($\sigma_T$) values were then calculated from the total resistance ($R_{total}$), cross-sectional area ($A$) and thickness ($l$) by using the following equation:

$$\sigma = \frac{l}{A.R_{total}} \tag{4}$$

The complex impedance spectra plots, which were constructed for temperatures of 250 °C, 400 °C and 800 °C in air, for the GDC-10 and GDC-20 samples sintered at 1400 °C are shown in Fig. 7. In Fig. 7a, two well-defined semicircular arcs, which denote the grain interior and grain boundary, are discernible. With increasing temperature (Fig. 7b), the first semicircle (the high-frequency arc) disappears and only the grain boundary and electrode arcs are visible. When the temperature increases (Fig. 7c), the grain interior and grain boundary resistances become frequency independent and only one semicircle, which refers to the electrode resistance, is visible.

At elevated temperatures in the approximate range of 700–800 °C, a single arc, which represents the electrode, was observed. This phenomenon is attributed to the effect on the spectra of inductances that was generated within the experimental apparatus [2]. The same trend was observed for all examined samples. The impedance behavior of the

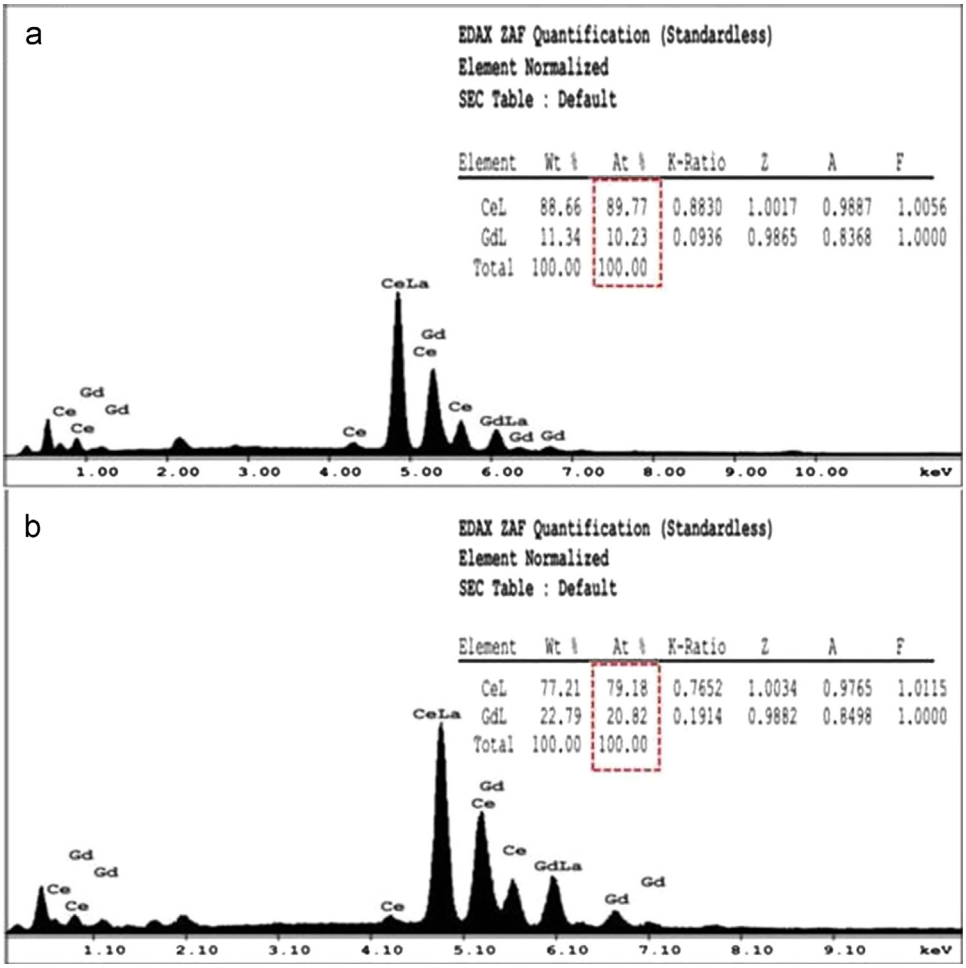


Fig. 6. EDX analysis of (a) GDC-10 and (b) GDC-20 samples.

GDC ceramic pellets was similar to the trend that is usually observed for polycrystalline ceramic materials, as documented in related research [25,33].

The temperature dependence of the ionic conductivities of GDC-10 and GDC-20 pellets that were sintered at 1100 °C, 1200 °C, 1300 °C, 1400 °C and 1500 °C are illustrated in Fig. 8; the total ionic conductivity values at 800 °C are tabulated in Table 2. The maximum ionic conductivity, which is comparable or better than the results of other studies, was measured for GDC-20/1400 °C at 800 °C with $3.25 \times 10^{-2}$ S cm$^{-1}$. For example, Rambabu et al. [34] reported a $2.4 \times 10^{-2}$ S cm$^{-1}$ ionic conductivity at 800 °C for GDC-20 sintered at 1400 °C. In addition, Dikmen et al. [35] measured $3.3 \times 10^{-4}$ S cm$^{-1}$ for GDC-10 and $5.1 \times 10^{-3}$ S cm$^{-1}$ for GDC-20 at 600 °C; whereas in this work, $5.8 \times 10^{-3}$ S cm$^{-1}$ and $7.6 \times 10^{-3}$ S cm$^{-1}$ conductivities were measured for GDC-10 and GDC-20 at 600 °C, respectively.

Note that the Arrhenius curve of doped ceria electrolyte cannot be fitted by a single straight line. This implies that

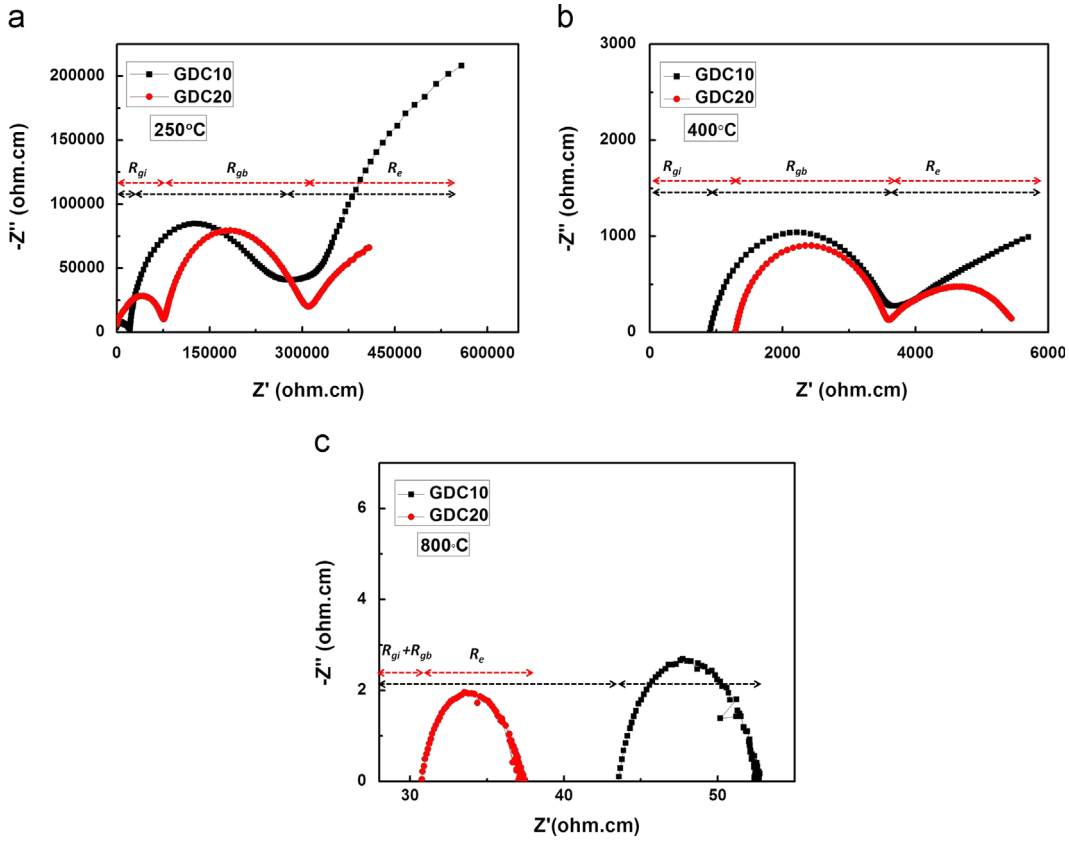


Fig. 7. Complex impedance spectra plots of GDC-10 and GDC-20 pellets sintered at 1400 °C, and measured at 250 °C, 400 °C and 800 °C in air. The grain interior, grain boundary and electrode contributions are represented as $R_{gi}$, $R_{gb}$ and $R_e$, respectively.

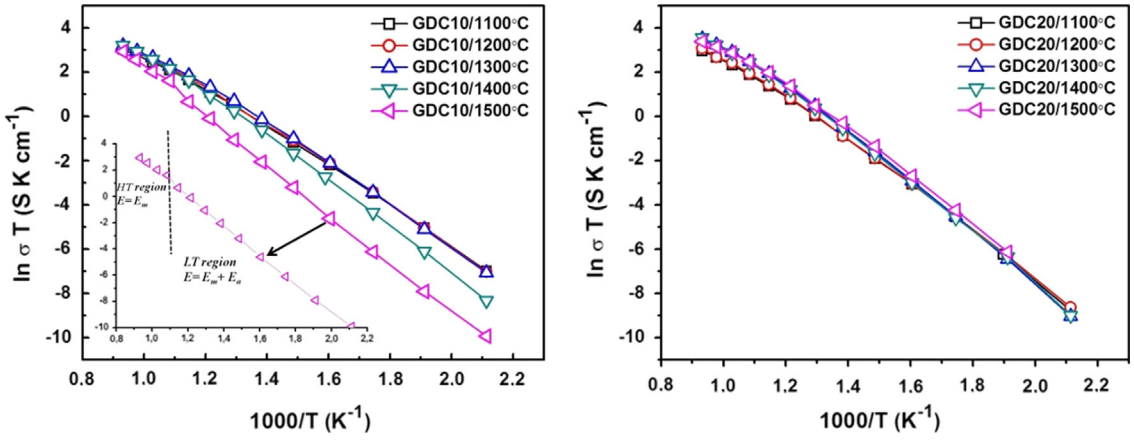


Fig. 8. Arrhenius plots of GDC-10 and GDC-20 samples.

Table 2
Ionic conductivities at 800 °C and activation energies of samples for both low temperature and high temperature regimes.

| Sintering temperature (°C) | Compositions | | | | | | | |
|---|---|---|---|---|---|---|---|---|
| | GDC-10 | Activation energy (eV) | | | GDC-20 | Activation energy (eV) | | |
| | Conductivity (S cm$^{-1}$) | LT | HT | $\Delta E$ | Conductivity (S cm$^{-1}$) | LT | HT | $\Delta E$ |
| 1100 | $1.89 \times 10^{-2}$ | 0.77 | 0.53 | 0.24 | $1.8 \times 10^{-2}$ | 0.90 | 0.61 | 0.29 |
| 1200 | $2.11 \times 10^{-2}$ | 0.78 | 0.53 | 0.25 | $2.01 \times 10^{-2}$ | 0.89 | 0.63 | 0.27 |
| 1300 | $2.25 \times 10^{-2}$ | 0.80 | 0.52 | 0.28 | $3.13 \times 10^{-2}$ | 0.97 | 0.59 | 0.39 |
| 1400 | $2.29 \times 10^{-2}$ | 0.88 | 0.60 | 0.28 | $3.25 \times 10^{-2}$ | 0.96 | 0.64 | 0.33 |
| 1500 | $1.75 \times 10^{-2}$ | 0.95 | 0.76 | 0.19 | $2.77 \times 10^{-2}$ | 0.91 | 0.51 | 0.40 |

the mechanism for conduction changes at a transition temperature [3]. According to the Arrhenius plots of all samples (shown in Fig. 8), there are two parts named LT (low temperature) and HT (high temperature) regimes in which the linearity of the plots change; and thus, the activation energy of the bulk, grain and overall conductivity change with increasing temperature.

Oxygen ionic conductivity in rare-earth doped ceria can be represented by the following equations:

$$\textit{at low temperatures } \sigma = \frac{\sigma_0}{T} e - \frac{(\Delta H_m + \Delta H_a)}{kT} \quad (5)$$

$$\textit{at high temperatures } \sigma = \frac{\boldsymbol{\sigma}_0}{T} e - \frac{(\Delta H_m)}{kT} \quad (6)$$

where $\Delta H_m$ is the migration enthalpy of the oxygen ions and $\Delta H_a$ is the association enthalpy of the dopant ion with the oxygen vacancies. Thus, the activation energy for conduction becomes the sum of activation energy for migration and association ($E = E_m + E_a$). Generally, it was suggested that at higher temperatures, the dopant-oxygen vacancy complex dissociates completely to free dopant cations and oxygen vacancy. The concentration of oxygen vacancy is independent of temperature and equivalent to the total concentration of dopant cations. Therefore, the migration enthalpy can be estimated from the slope of Arrhenius plots in the higher temperature regime. The association enthalpy can be calculated from the differences of the slopes at higher and lower temperature regimes [36–38]. The results are provided in Table 2.

The $\Delta E$ column denotes association enthalpy of the dopant ion–oxygen vacancy complex because $E_{LT} = E_a + E_m$ and $E_{HT} = E_m$. With an increasing Gd content from 10% to 20%, the association enthalpies increased almost 1.5 times due to the interaction of Gd ions and oxygen vacancy. Although the migration enthalpy also increased with increased Gd content, there is no significant difference in Gd content. The overall LT activation energy values were approximately 0.8–0.9 eV for both groups, which is consistent with reported studies [6,25].

The ionic conductivity of the GDCs increased when sintering temperature increased, up to 1400 °C. Conversely, for sintering 1500 °C, the ionic conductivities of the samples decreased significantly for both groups. Lenka et al. [39] reported that the bulk conductivity increases with an increase in grain size, and grain boundary conductivity decreases with an increase in grain size. (We also observed the same trend in this study.) Due to these results, there is a competitive situation between an increase in bulk conductivity and a decrease in grain boundary conductivity. Above a critical temperature, the effect of grain boundary becomes more dominant for total conductivity. Therefore, the reverse V-type behavior is acceptable. When the GDC-10 and GDC-20 samples that were sintered at 1400 °C (because the results for 1400 °C are the best for both groups) were compared at lower temperatures (250 °C), the lattice conductivity (grain interior) of GDC-10 was 3.5 times the lattice conductivity of GDC-20 for the 1400 °C samples. Although the grain boundary resistance of GDC-10 is higher than the grain boundary resistance of GDC-20 due to a lower grain interior ($R_i$) resistance, the observed total conductivity of GDC-10 is higher than the observed total conductivity of GDC-20. At 400 °C, the difference in grain interior resistance between the two samples decreased and the two samples exhibited nearly equivalent total conductivities. At 800 °C, the grain interior ($R_{gi}$) and grain boundary ($R_{gb}$) resistances are not discrete; only the total conductivity can be calculated. At this temperature, the conductivity of GDC-20 was 1.4 times higher than the conductivity of GDC-10. Research findings have claimed that for the Gd dopant content, the composition $x = 0.1$ yields the maximum lattice conductivity, but above 400 °C the composition $x = 0.2$ yields the maximum lattice conductivity [28]. This behavior can be attributed to the difference in activation energy between the two samples. Low activation energy typically indicates low-temperature dependency; the GDC-20/1400 °C sample contains higher activation energy (both low and high temperature regions) than the GDC-10/1400 °C sample.

For the compositions with $x = 0.1$ and $x = 0.2$, gadolinia-doped ceria is one of the most frequently used electrolytes for IT-SOFCs [40]. However, some confusion exists over the selection of optimal GDC electrolyte composition. The GDC-20 electrolyte has demonstrated a better total ionic conductivity than the GDC-10 electrolyte, as described in the study [41–45].

## 4. Conclusion

The polyol processing of gadolinium and cerium acetate precursors leads to the production of nanocrystalline GDC-10 and GDC-20 powders after calcination at 500 °C. The XRD patterns of the samples prepared with the polyol method exhibited the fluorite structure of $CeO_2$. The effect of sintering temperature and concentration of Gd on the properties of GDC were thoroughly studied. After sintering, the nano-sized gadolinia-doped ceria pellets achieved over 95% of the theoretical density at approximately 1300 °C.

According to the electrochemical impedance spectroscopy results, GDC-10/1400 °C exhibited a total conductivity of $2.29 \times 10^{-2}$ S cm$^{-1}$ and GDC-20/1400 °C exhibited a total conductivity of $3.25 \times 10^{-2}$ S cm$^{-1}$ at 800 °C. $Gd_{0.2}Ce_{0.8}0_{1.9}$ is a more promising electrolyte for IT-SOFC based on our results.

This paper discusses one of the first studies to use the polyol method to obtain electrolyte materials with detailed conductivity results. To obtain ceria-based electrolytes with higher ionic conductivity, additional studies will be performed.

## Acknowledgments

This study was supported by Istanbul University through Project T.R. of The Turkish Prime Ministry State Planning Organization (DPT) with Project Number of 2008K121000, and by The Research Fund of Istanbul University with grant numbers 26803 and 27829.

## References

[1] J. Luo, R.J. Ball, R. Stevens, Gadolinia doped ceria/yttria stabilised zirconia electrolytes for solid oxide fuel cell applications, Journal of Materials Science 39 (2004) 235–240.
[2] R.O. Fuentes, R.T. Baker, Synthesis and properties of gadolinium-doped ceria solid solutions for IT-SOFC electrolytes, International Journal of Hydrogen Energy 33 (2008) 3480–3484.
[3] S. Zha, C. Xia, G. Meng, Effect of Gd (Sm) doping on properties of ceria electrolyte for solid oxide fuel cells, Journal of Power Sources 115 (2003) 44–48.
[4] L.D. Jadhav, M.G. Chourashiya, K.M. Subhedar, A.K. Tyagi, J.Y. Patil, Synthesis of nanocrystalline Gd doped ceria by combustion technique, Journal of Alloys and Compounds 470 (2009) 383–386.
[5] H.J. Park, G.M. Choi, Oxygen permeability of gadolinium-doped ceria at high temperature, Journal of the European Ceramic Society 24 (2004) 1313–1317.
[6] L.D. Jadhav, S.H. Pawar, M.G. Chourashiya, Effect of sintering temperature on structural and electrical properties of gadolinium doped ceria ($Ce_{0.9}Gd_{0.1}O_{1.95}$), Bulletin of Materials Science 30 (2) (2007) 97–100.
[7] S. Wang, T. Kobayashi, M. Dokiya, T. Hashimoto, Electrical and ionic conductivity of Gd-doped Ceria, Journal of the Electrochemical Society 147 (10) (2000) 3606–3609.
[8] M. Hirano, E. Kato, Hydrothermal synthesis of cerium (IV) oxide, Journal of the American Ceramic Society 79 (3) (1996) 777–780.
[9] Y.C. Zhou, M.N. Rahman, Hydrothermal synthesis and sintering of ultrafine $CeO_2$ powders, Journal of Materials Research 8 (1993) 1680.
[10] N. Uekewa, M. Ueta, Y.J. Wu, K. Kakewa, Chemistry Letters 8 (2002) 854.
[11] H.I. Chen, H.Y. Chang, Homogeneous precipitation of cerium dioxide nanoparticles in alcohol/water mixed solvents, Colloids Surface A 242 (2004) 61.
[12] G.S. Wu, T. Xie, X.Y. Yuan, B.C. Cheng, L.D. Zhang, An improved sol–gel template synthetic route to large-scale $CeO_2$ nanowires, Materials Research Bulletin 39 (2004) 1023.
[13] C.R. Xia, M.L. Liu, Microstructures, conductivities, and electrochemical properties of $Ce_{0.9}Gd_{0.1}O_2$ and GDC-Ni anodes for low-temperature SOFCs, Solid State Ionics (2002) 152–423.
[14] M.M.A. Sekar, S.S. Manoharan, K.C. Patil, Combustion synthesis of fine-particle ceria, Journal of Materials Science Letters 9 (1990) 1205.
[15] J. Chandradass, B. Nam, K.H. Kim, Fine tuning of gadolinium doped ceria electrolyte nanoparticles via reverse microemulsion process, Colloids Surface A 348 (2009) 130–136.
[16] R.A. Rocha, E.N.S. Muccillo, Physical and chemical properties of nanosized powders of gadolinia-doped ceria prepared by the cation complexation technique, Materials Research Bulletin 38 (2003) 1979–1986.
[17] A. Gondolini, E. Mercadelli, A. Sanson, S. Albonetti, L. Doubova, S. Boldrini, Microwave-assisted synthesis of gadolinia-doped ceria powders for solid oxide fuel cells, Ceramics International 37 (2011) 1423–1426.
[18] T. Karaca, T.G. Altınçekiç, M.F. Öksüzömer, Synthesis of nanocrystalline samarium doped $CeO_2$(SDC) powders as a solid electrolyte by using a simple solvothermal route, Ceramics International 36 (2010) 1101–1107.
[19] B.C.H. Steele, Appraisal of $Ce_{1-y}$ $Gd_y$ $O_{2-y/2}$ electrolytes for IT-SOFC operation at 500 °C, Solid State Ionics 129 (2000) 95–110.
[20] J. Kilner, Fast oxygen transport in acceptor doped oxides, Solid State Ionics 123 (2000) 13–23.
[21] K.R. Reddy, K. Karan, Sinterability, mechanical, microstructural, and electrical properties of gadolinium-doped ceria electrolyte for low-temperature solid oxide fuel cells, Journal of Electroceramics 15 (2005) 45–56.
[22] L.E. Smart, E.A. Moore, Solid State Chemistry: An Introduction, 3rd Edition, CRC Taylor and Francis Group, 2005.
[23] X. Guan, H. Zhou, Z. Liu, Y. Wang, J. Zhang, High performance $Gd^{3+}$ and $Y^{3+}$ co-doped ceria-based electrolytes for intermediate temperature solid oxide fuel cells, Materials Research Bulletin 43 (2008) 1046–1054.
[24] J. Li, T. Ikegami, T. Mori, Low temperature processing of dense samarium-doped $CeO_2$ ceramics: sintering and grain growth behaviors, Acta Materialia 52 (2004) 2221–2228.
[25] C. Veranitisagul, A. Kaewvilai, W. Wattanathana, N. Koonsaeng, E. Traversa, A. Laobuthee, Electrolyte materials for solid oxide fuel cells derived from metal complexes: Gadolinia-doped ceria, Ceramics International 38 (2012) 2403–2409.
[26] T. Suzuki, I. Kosacki, H.U. Anderson, Microstructure–electrical conductivity relationships in nanocrystalline ceria thin films, Solid State Ionics 151 (2002) 111–121.
[27] M.G. Chourashiya, J.Y. Patil, S.H. Pawar, L.D. Jadhav, Studies on structural, morphological and electrical properties of $Ce_{1-x}Gd_xO_{2-(x/2)}$, Materials Chemistry and Physics 109 (2008) 39–44.
[28] Z. Tianshu, P. Hing, H. Huang, J. Kilner, Ionic conductivity in the $CeO_2$–$Gd_2O_3$ system ($0.05 \le Gd/Ce \le 0.4$) prepared by oxalate coprecipitation, Solid State Ionics 148 (2002) 567–573.
[29] E. Barsoukov, J.R. Macdonald, Impedance Spectroscopy Theory, Experiment, and Applications, 2nd Edition, Wiley, 2005.
[30] J.E. Bauerle, Study of solid electrolyte polarization by a complex admittance method, Journal of Physics and Chemistry of Solids 30 (12) (1969) 2657–2670.
[31] T.S. Zhang, J. Ma, Y.Z. Chen, L.H. Luo, L.B. Kong, S.H. Chan, Solid State Ionics 177 (2006) 1227–1235.
[32] D.Y. Wang, A.S. Nowick, Journal of Solid State Chemistry 35 (1980) 325–333.

[33] R.S. Torrens, N.M. Sammes, G.A. Tompsett, Characterisation of $(CeO_2)_{0.8}$ $(GdO_{1.5})_{0.2}$ synthesised using various techniques, Solid State Ionics 111 (1998) 9–15.

[34] B. Rambabu, S. Ghosh, H. Jena, Novel wet-chemical synthesis and characterization of nanocrystalline $CeO_2$ and $Ce_{0.8}Gd_{0.2}O_{1.9}$ as solid electrolyte for intermediate temperature solid oxide fuel cell (IT-SOFC) applications, Journal of Materials Science 41 (2006) 7530–7536.

[35] S. Dikmen, P. Shuk, M. Greenblatt, H. Gocmez, Hydrothermal synthesis and properties of $Ce_{1-x}$ $Gd_xO_{2-\delta}$ solid solutions, Solid State Science 4 (2002) 585–590.

[36] J.A. Kilner, B.C.H. Steele, in: O.T. Sorensen (Ed.), Nonstoichiometric Oxides, Academic Press, London, 1981, p. 233 .S.C.

[37] S.C. Singhal, K. Kendall, High Temperature Solid Oxide Fuel Cells: Fundamentals, Design, and Applications, Elsevier, Oxford, 2003.

[38] H. Özdemir, V. Sarıboğa, M.A. Faruk Öksüzömer, M.A. Gürkaynak, Preparation and characterization of Ca-Sm-Ce mixed oxides via cellulose templating method for solid oxide fuel cell applications, Journal of Power Sources 219 (2012) 155–162.

[39] R.K. Lenka, T. Mahata, A.K. Tyagi, P.K. Sinha, Influence of grain size on the bulk and grain boundary ion conduction behavior in gadolinia-doped ceria, Solid State Ionics 181 (2010) 262–267.

[40] T. Mori, R. Buchanan, D.R. Ou, F. Ye, T. Kobayashi, J.D. Kim, J. Zou, J. Drennan, Jouranl of Solid State Electrochemistry 12 (2008) 841–849.

[41] Z. Li, T. Mori, P. Yan, Y. Wu, Z. Li, Preparation and performance of intermediate-temperature fuel cells based on Gd-doped ceria electrolytes with different compositions, Materials of Science and Engineering B 177 (2012) 1538–1541.

[42] V.V. Kharton, F.M.B. Marques, A. Atkinson, Solid State Ionics 174 (2004) 135–149.

[43] S. Uhlenbruck, T. Moskalewicz, N. Jordan, H.J. Penkalla, H.P. Buchkremer, Solid State Ionics 180 (2009) 418–423.

[44] M. Mogensen, N.M. Sammes, G.A. Tompsett, Physical, chemical and electrochemical properties of pure and doped ceria, Solid State Ionics 129 (2000) 63–94.

[45] B.C.H. Steele, in: T. Takahashi (Ed.), High Conductivity Solid Ionic Conductors, Recent Trends and Applications, World Scientific, London, 1989, p. 402.